# Asymptotic normalization coefficients from transfer reactions and *R*-matrix analysis of direct capture in the $^{22}$Ne($p$, $\gamma$) $^{23}$Na reaction

Rajkumar Santra,[1,2] Suprita Chakraborty,[3] and Subinit Roy[1,*]
[1]*Saha Institute of Nuclear Physics, 1/AF, Bidhan Nagar, Kolkata 700064, India*
[2]*Homi Bhabha National Institute, Anushaktinagar, Mumbai 400094, India*
[3]*Belgachia Aswini Dutta Vidyapith for Girls High, Belgachia Howrah, India*

(Received 13 September 2019; revised manuscript received 19 December 2019; accepted 14 January 2020; published 6 February 2020)

The $^{22}$Ne($p$, $\gamma$) $^{23}$Na reaction in the Ne-Na cycle plays an important role in the production of the only stable sodium isotope $^{23}$Na. This nucleus is processed by the Ne-Na cycle during hot bottom burning (HBB) in the asymptotic giant branch (AGB) stage of low metallicity intermediate mass stars ($4M_\odot \leqslant M \leqslant 6M_\odot$). Recent measurements have addressed the uncertainty in the thermonuclear reaction rate of this reaction at relevant astrophysical energies through the identification of low lying resonances at $E_p = 71$, 105, 156.2, 189.5, and 259.7 keV. In addition, precise measurements of the low energy behavior of nonresonant capture have been performed and the contribution of the subthreshold resonance at 8664 keV excitation in $^{23}$Na has been established. Here we present a systematic *R*-matrix analysis of direct capture to the bound states and the decay of the subthreshold resonance at 8664 keV to the ground state of $^{23}$Na. A finite-range distorted-wave Born approximation (FRDWBA) calculation has been performed for the $^{22}$Ne($^3$He, $d$) $^{23}$Na transfer reaction data to extract the asymptotic normalization coefficients (ANCs) required to estimate the nonresonant capture cross sections or astrophysical *S*-factor values in the *R*-matrix analysis. Simultaneous *R*-matrix analysis constrained with ANCs from transfer calculations reproduced the astrophysical *S*-factor data over a wide energy window. The value $S_{tot}^{DC}(0) = 48.8 \pm 9.5$ keV b compares well with the result of Ferraro *et al.* and has a lower uncertainty. The resultant thermonuclear reaction is slightly larger in the $0.1 \leqslant T \leqslant 0.2$ GK temperature range but otherwise in agreement with Ferraro *et al.*

DOI: 10.1103/PhysRevC.101.025802

## I. INTRODUCTION

The proton capture reaction $^{22}$Ne($p$, $\gamma$) $^{23}$Na of the neon-sodium cycle of hydrogen burning in stars consumes $^{22}$Ne, a seed nucleus for neutron production for *s*-process nucleosynthesis, and converts it to $^{23}$Na, the only stable isotope of sodium. The reaction occurs in the convective envelop of massive ($M \geqslant 4M_\odot$) asymptotic giant branch (AGB) stars at temperature $T \approx 1.0 \times 10^8$ K ($T_9 \approx 0.1$). In more massive stars ($M \geqslant 50M_\odot$), the reaction takes place in the surface layer along with the carbon-nitrogen-oxygen (CNO) and magnesium-aluminium (Mg-Al) cycles of hydrogen burning at temperatures up to $T_9 \approx 0.8$) [1–4]. Since oxygen is destroyed in the CNO cycle and Na is produced in the Ne-Na cycle, the reaction $^{22}$Ne($p$, $\gamma$) $^{23}$Na is said to be responsible for the observed anticorrelation in surface oxygen and sodium abundances in galactic globular clusters [5–7].

The rate of the $^{22}$Ne($p$, $\gamma$) $^{23}$Na capture reaction in the relevant astrophysical energy domain is dominated by the contributions of several low energy resonances in $^{23}$Na and a slowly varying off-resonant capture contribution. Precision measurements have been carried out in recent years to identify and confirm the important low energy resonances and determine the resonance strengths [8–13]. The studies helped resolve the discrepancy that existed between the recommended value of the reaction rate from the NACRE I compilation [14] and those determined in Refs. [15–17] in AGB stars in the temperature window $0.08 \leqslant T \leqslant 0.25$ GK.

The measurement of Ferraro *et al.* [13], besides providing stringent upper limits for the strengths of low energy resonances at proton beam energies of 71 and 105 keV, also reported a slowly varying nonresonant component having a significant contribution in the same temperature window. Prior to this work, the nonresonant, direct capture (DC) processes in the $^{22}$Ne($p$, $\gamma$) reaction to the bound states of $^{23}$Na and their contributions to low energy behavior of the astrophysical *S* factor were studied in Refs. [12,18,19]. Earlier studies used a constant value of $S_{DC}(E) = 62.0$ keV b obtained by Görres *et al.* [19] from their measurement of higher energy direct capture data. Kelly *et al.* [12] measured the direct capture cross section at a single proton beam energy of 425 keV and maintained the same value for $S_{DC}$ ($E =$ 0 MeV). Ferraro *et al.* in a subsequent high statistics and low background measurement extended the nonresonant capture cross section to 310, 250, 205, and 188 keV proton beam energies. Their analysis yielded $S_{DC}(0) = 50 \pm 12$ keV b. However, the authors observed a distinct rise in the low energy astrophysical *S*-factor data and showed that the rise in the off-resonant astrophysical *S* factor is a consequence of capture to the subthreshold state at 8664 keV excitation in $^{23}$Na.

*subinit.roy@saha.ac.in

 

TABLE I. Present status of $^{22}$Ne$(p,\gamma)$ $^{23}$Na reaction rate.

| Source | $S_{DC}(0)$ (keV b) | Reaction rate ($T_9 \approx 0.1$) (cm$^3$ mol$^{-1}$ s$^{-1}$) |
|---|---|---|
| Rolfs 1975 [18] | $67 \pm 19$ | |
| Gorres 1983 [19] | 62 | |
| Hale 2001 [15] | | $5.07 \times 10^{-9}$ |
| Sallaska 2013 [17] | | $5.52 \times 10^{-9}$ |
| Cavanna 2015 [8] | | $6.6 \times 10^{-8}$ |
| Depalo 2016 [9] | | $2.7 \times 10^{-8}$ |
| Kelly 2017 [12] | 62 | $4.31 \times 10^{-8}$ |
| Ferraro 2018 [13] | $50 \pm 12$ | $5.07 \times 10^{-8}$ |

In Table I, the reaction rates at $T \approx 0.1$ GK found in the literature are tabulated. The contributions of $S_{DC}(0)$ in the total astrophysical $S$ factor at zero energy are also shown. A recent measurement by Ferraro *et al.* reported a mean rate which is about 18% higher than the rate predicted by Kelly *et al.* but 46% higher than the rate estimated by Depalo *et al.* [9]. Also the value of $S_{DC}(0)$ obtained by Ferraro *et al.* is relatively lower than that by Kelly *et al.*. Again, Ferraro *et al.* obtained a value of $13 \pm 5$ keV b from their analysis for $S_{DC}^{GS}$ that is considerably higher than the value used by Görres *et al.* [19]. Although the direct capture cross section is not significantly high in contribution [12], we intended to perform a consistent analysis of the direct capture data including the data from the recent measurement of Ferraro *et al*.

In this context, we reported a detailed analysis of the available $S$-factor data for nonresonance capture to the ground state (GS) and 440, 2392, 2982, 6318, 6918 and 8664 keV excited states of the $^{23}$Na nucleus, as indicated in Fig. 1, and the total nonresonant $S$-factor data within the framework of $R$-matrix model. The aim is to investigate the energy dependence of the total off-resonance astrophysical $S$ factor including the contribution of the broad, subthreshold ($-130$ keV) state at 8664 keV and to extend the curve to still lower energies of astrophysical interest. We constrained the $R$-matrix calculation of the direct capture contribution using the spectroscopic information extracted from the reanalysis of available data from the literature on the one proton transfer reaction on the nucleus $^{22}$Ne. The total reaction rate is then estimated from the calculated reaction rate due to the off-resonance process and the measured strengths of important low energy resonances in $^{23}$Na except for the state with resonance energy 151 keV. Experimental evidence shows that the state at 8945 MeV excitation corresponding to resonance energy 151 keV is actually a doublet with capture of $d$ and $f$ waves populating the states. A reanalysis of the proton transfer reaction to the unbound 8945 MeV state ($Q_p = 8794$ MeV) was performed to extract the resonance strengths indirectly. The resultant reaction rate up to $T = 1.0$ GK was compared with the recent estimations of Ferraro *et al*.

## II. ANALYSIS

The model calculation progressed in two steps. In the first step, the data from the $^{22}$Ne($^3$He, $d$) $^{23}$Na transfer reaction to the bound states of $^{23}$Na have been reanalyzed to extract the asymptotic normalization coefficients (ANCs) of the states. The second part constitutes $R$-matrix calculation for the data of direct capture to those bound states using the ANCs from the first part of the calculation.

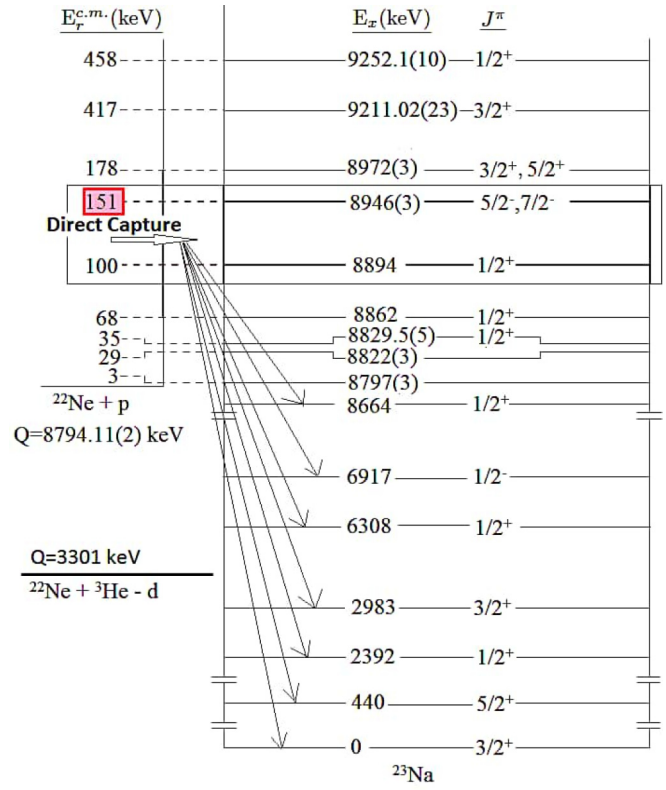


FIG. 1. Level scheme of $^{23}$Na. The black box in the figure corresponds to Gamow window for $T_9 = 0.1$.

### A. Finite-range DWBA analysis and extraction of ANC

A finite-range distorted-wave Born approximation (FRDWBA) calculation was performed for the angular distribution data of the $^{22}$Ne($^3$He, $d$) $^{23}$Na one-proton stripping reaction from Refs. [15,20]. In the FRDWBA model, conventionally the experimental cross section of a transfer reaction $A + a(= b + x) \rightarrow B(= A + x) + b$ (where $x$ is the transferred particle)

TABLE II. Spectroscopic factors and asymptotic normalization coefficients (ANCs) for the first seven states of $^{23}$Na

| $E_x$ (keV) | $J^\pi$ | $nl_j$ | $C^2S$[a] Present | $C^2S$ Ref. [20] | $b$ (fm$^{-1/2}$) | ANC (fm$^{-1/2}$) |
|---|---|---|---|---|---|---|
| GS | $3/2^+$ | $1d_{3/2}$ | $0.082 \pm 0.012$ | 0.08 | 6.86 | $1.96 \pm 0.5$ |
| 440 | $5/2^+$ | $1d_{5/2}$ | $0.38 \pm 0.08$ | 0.35 | 7.62 | $4.69 \pm 0.8$ |
| 2392 | $1/2^+$ | $2s_{1/2}$ | $0.26 \pm 0.05$ | 0.25 | 17.56 | $8.8 \pm 1.6$ |
| 2982 | $3/2^+$ | $1d_{3/2}$ | $0.35 \pm 0.04$ | 0.32 | 4.38 | $2.59 \pm 0.87$ |
| 6308 | $1/2^+$ | $2s_{1/2}$ | $0.14 \pm 0.02$ | 0.13 | 11.14 | $4.16 \pm 0.79$ |
| 6917 | $1/2^-$ | $2p_{1/2}$ | $0.18 \pm 0.04$ | 0.15 | 7.27 | $3.1 \pm 0.7$ |

[a]Geometry parameters of bound state potential $a_0 = 0.6$, $r_0 = 1.26$.

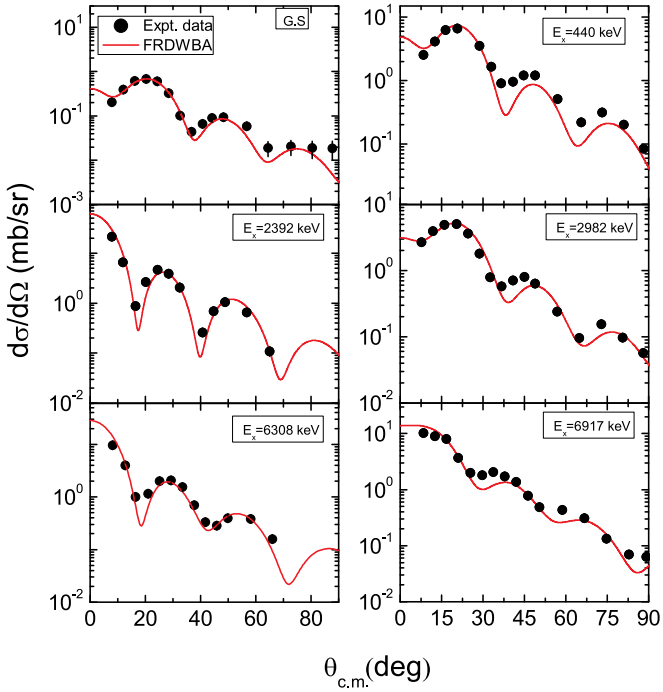


FIG. 2. Transfer angular distributions fitted with FRDWBA model calculation.

is compared with the calculated cross section by the relation

$$\left(\frac{d\sigma}{d\Omega}\right)_{\rm exp} = (C^2S)_{bx}(C^2S)_{Ax}\left(\frac{d\sigma}{d\Omega}\right)_{\rm mod}, \qquad (1)$$

where $C^2S_{bx}$ is the product of spectroscopic factor $S_{bx}$ and isospin Clebsh-Gordon coefficient $C^2_{bx}$ of the $b+x$ configuration in projectile $a$, and $C^2S_{Ax}$ is that for the $A+x$ configuration in residual nucleus $B$. $(\frac{d\sigma}{d\Omega})_{\rm mod}$ is the cross section obtained from the model calculation.

To extract the spectroscopic factors from data, a finite-range distorted-wave Born approximation (FRDWBA), using the code FRESCO (ver. 2.9) [21], was performed. Angular distribution data, measured at 15 MeV incident energy, for transfer to the ground state and 440, 2392, 2982, 6308, 6917 keV exited states were taken from Ref. [20]. The data from Ref. [15], measured with a 20 MeV $^3$He beam, was used for transfer to the subthreshold state of $^{23}$Na at 8664 keV excitation energy.

In the reanalysis of 15 MeV data within the FRDWBA framework, the optical model potential parameters for entrance and exit channels were taken from Ref. [20]. Standard Woods-Saxon form was used for the potentials. The shape parameters for the bound sate potentials related to $^{22}$Ne $+p$ and $d+p$ systems are from Refs. [20] and [22], respectively. The strengths of the bound state potentials were varied to get the binding energies of the states of the composite nuclei.

The model calculations reproduced quite well the angular distributions for transfer to the ground state and 440, 2392, 2982, 6308, 6917 keV exited states of $^{23}$Na shown in Fig. 2. While extracting the spectroscopic factors of the states of $^{23}$Na, the spectroscopic factor $C^2S_{dp}$ for $^3$He was taken as 1.092, a value that was derived for the $^3$He ground state with $d+p$ configuration using the method reported in Ref. [22]. The resultant spectroscopic factors of $^{23}$Na states are shown in Table II. The values obtained from the present FRDWBA analysis match well with those reported from the zero-range DWBA calculation in Ref. [20].

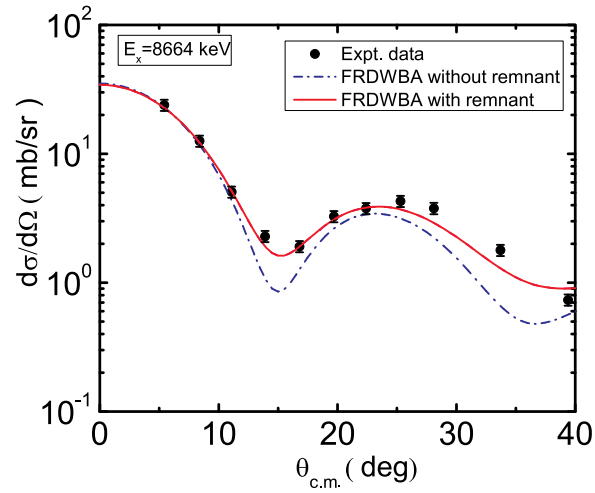


FIG. 3. DWBA fit to angular distribution data of Power *et al.* [20] for the state $E_x = 8664$ keV. The line represents calculated cross section

### *1. DWBA analysis of the $^{22}$Ne($^3$He, $d$) reaction for the $E_x$ = 8664 keV state*

The excited state 8664 keV of $^{23}$Na is 130 keV below the proton threshold at 8794 keV. Capture through this subthreshold resonance controls the low energy behavior of the astrophysical $S$ factor of the $^{22}$Ne$(p,\gamma)$ reaction. To extract the spectroscopic factor of this state we again performed a FRDWBA calculation for the transfer reaction $^{22}$Ne($^3$He, $d$) at 20 MeV with the data from Ref. [15]. Potential parameters used to obtain the transfer angular distribution are given in Table III. It has been observed that, unlike the more deeply bound states in $^{23}$Na, a complex remnant term is required to obtain a very good overall fit to the angular distribution data. The parameters of $d+^{22}$Ne core-core potential are also given in Table III. The resultant fit is shown by solid red line in Fig. 3. The blue dashed-dotted line represents the FRDWBA calculation without the remnant term. Improvement in the fit is quite remarkable. In column 5 of Table IV we show the extracted spectroscopic factors. The values obtained from the present work are very close to the values reported in Refs. [15,19].

### *2. Extraction of ANCs*

The spectroscopic factors so determined include the effect of the nuclear interior and measure the many-body effect in the transfer reaction process. They depend on the choice of the potentials, more sensitively on the geometry parameters of the bound state potential used to describe a particular configuration. In low energy radiative capture reactions, instead of spectroscopic factor, the asymptotic normalization coefficient or ANC is more relevant a quantity. The ANC measures the

TABLE III. Potential parameters for $^{22}$Ne($^{3}$He, $d$) $^{23}$Na ($E_x = 8664$ keV), $E_{\rm lab} = 20$ MeV [15].

| Channel | $V_r$ (MeV) | $r_r$ (fm) | $a_r$ (fm) | $W_i$ (MeV) | $W_D$ (MeV) | $r_i = r_D$ (fm) | $a_i = a_D$ (fm) | $V_{so}$ (MeV) | $r_{so}$ (fm) | $a_{so}$ (fm) | $r_c$ (fm) |
|---|---|---|---|---|---|---|---|---|---|---|---|
| $^{3}$He + $^{22}$Ne | Ref. [15] | | | | | | | | | | |
| $d$ + $^{23}$Na | Ref. [15] | | | | | | | | | | |
| $d$ + $^{22}$Ne | 88.0 | 1.17 | 0.73 | 0.24 | 35.8 | 1.33 | 0.73 | 13.85 | 1.07 | 0.66 | 1.33 |
| $d + p$ | [a] | 1.25 | 0.65 | | | | | 6.2 | 1.25 | 0.65 | 1.30 |
| $p$ + $^{22}$Ne | Ref. [15] | | | | | | | | | | |

[a]Varied to match separation energy.

amplitude of the tail of the overlap between the bound state wave unctions of initial and final nuclei. It is related to the spectroscopic factor of the two-body configuration as

$$C^2S_{J_f l_f} = \left(\frac{C_{J_f l_f}}{b_{l_f j_f}}\right)^2, \tag{2}$$

where $C^2S_{J_f l_f}$ is the spectroscopic factor of the configuration in the composite nucleus with total spin $J_f$. The relative orbital angular momentum and spin of the two clusters in the final bound state are denoted by $l_f$ and $j_f$. $C_{J_f l_f}$ is the corresponding ANC and $b_{l_f j_f}$ is the single-particle asymptotic normalization constant (SPANC) with $l_f$ and $j_f$ quantum numbers of the bound state orbital used in the DWBA calculation. The SPANC $b$ is expressed in terms of the bound state wave function of the composite nucleus [23] as

$$b(r_0, a_0) = \frac{u(r, r_0, a_0)}{W_{-n,l+1/2}(2\kappa r)}, \tag{3}$$

in the asymptotic radial region. $W_{-n,l+1/2}(2\kappa r)$ is the Whittaker function, $\kappa = \sqrt{2\mu\epsilon}$ is the wave number, and $\mu, \epsilon, R_N$ are the reduced mass, binding energy, and the nuclear interaction radius, respectively for the bound state of the final nucleus. Both the bound state wave function and the Whittaker function have similar radial fall-off in the asymptotic region. The parameters $r_0$ and $a_0$ are the radius parameter and diffuseness of the Woods-Saxon potential generating the required bound state wave function. In all cases the strength of the bound state potential is obtained by reproducing the binding energy of the state.

In the present work, the value $b_{l_f j_f}$ associated with each bound state has been obtained from the best fit ratio value using Eq. (3) for the region beyond the radius $R_N = 5.5$ fm. Like the spectroscopic factor, SPANC $b$ also depends on the choice of potential parameters. But the variations of the two quantities with the geometry parameters of the bound state potential are opposite in nature. Hence, the product of these two quantities that gives the required ANC remains constant with the change of potential parameters for a peripheral reaction. Thus, for a pure peripheral condition the variation of spectroscopic factor should be proportional to the inverse square of the SPANC value [24] from Eq. (3). In Fig. 4 we show the plots of variation of $C^2S$ as a function of SPANC $b$ for the 8664 keV subthreshold state and deeply bound 440 keV state. The error shown in the figure for $C^2S$ includes the uncertainty of DWBA fit to the angular distribution data for a particular SPANC value obtained for the chosen $r_0$ and $a_0$ parameters of the bound state potential and the experimental

TABLE IV. Spectroscopic factors and asymptotic normalization coefficient (ANC) of the 8664 keV state of $^{23}$Na.

| $E_x$ (MeV) | $J^\pi$ | $l_p$ | $nl_j$ | $C^2S$ | $b$ (fm$^{-1/2}$) | ANC (fm$^{-1/2}$) |
|---|---|---|---|---|---|---|
| 8664[a] | $1/2^+$ | 0 | $2s_{1/2}$ | $0.32 \pm 0.05$ | 252[b] | $143.7 \pm 15.2$ |
| | | | | 0.29 [15] | | |
| | | | | 0.3 [19] | | |
| | | | | $0.42 \pm 0.08$ [13] | | |
| | | | | $0.58 \pm 0.08$ [25] | | |

[a]Subthreshold state. $E_r = -130$ keV.
[b]Geometry parameters of bound state potential $a_0 = 0.69$, $r_0 = 1.17$.

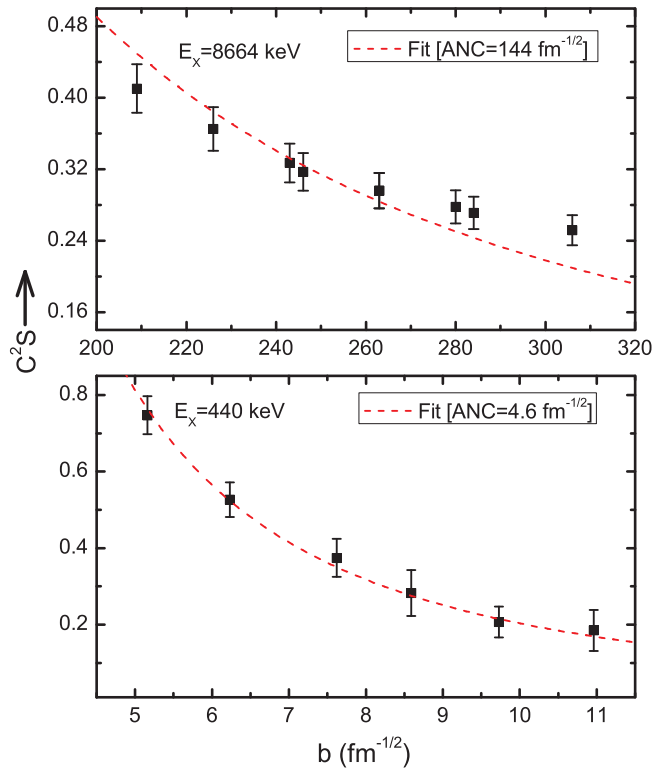


FIG. 4. Variation of spectroscopic factor with single particle ANC for 8664 MeV (top panel) and 440 MeV (lower panel) states.

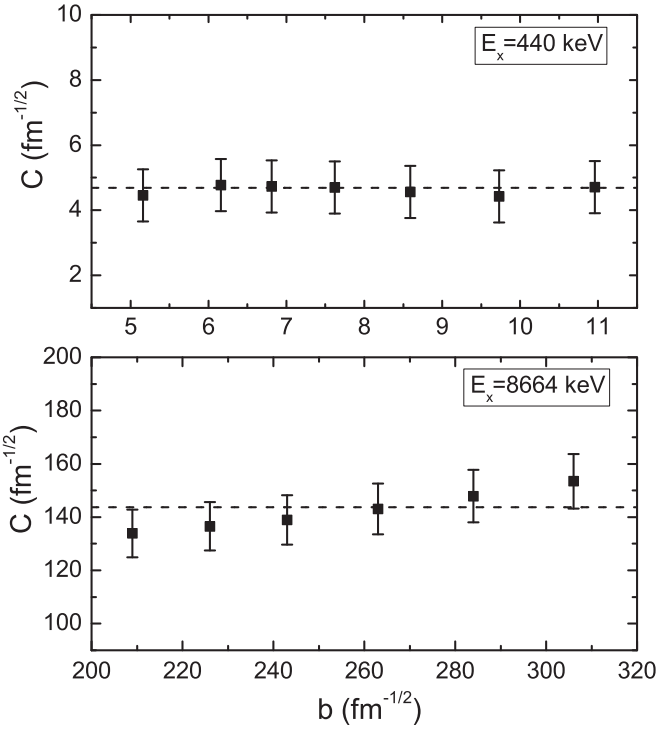


FIG. 5. Variation of ANC [$C$ (fm$^{-1/2}$)] as a function of SPANC [$b$ (fm$^{-1/2}$)] for 440 keV (top panel) and 8664 keV (bottom panel) states.

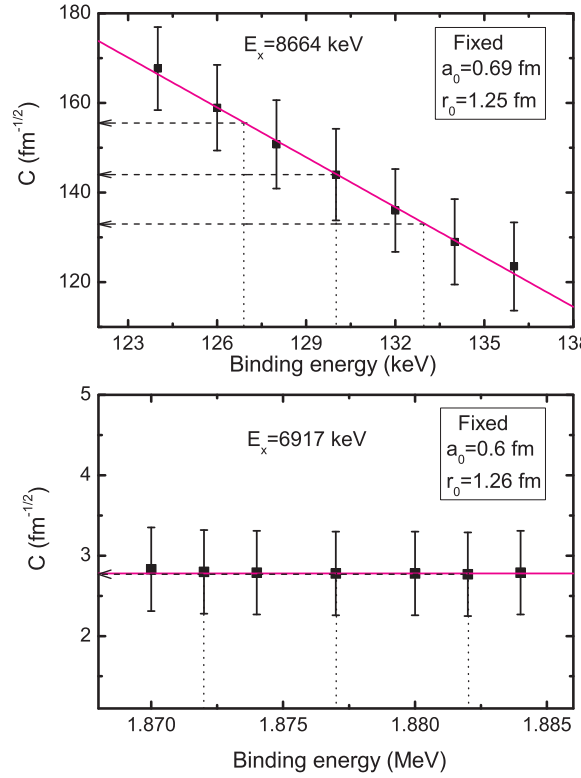


FIG. 6. Variation of ANC [$C$ (fm$^{-1/2}$)] as a function of binding energy for 8664 keV (top panel) and 6917 keV (bottom panel) states for fixed geometry parameters of the bound state potential.

error of individual cross section data. The radius and diffuseness parameters were changed in small steps to generate the corresponding SPANC value. The fits with inverse square function to the extracted data ensure the peripheral nature of the process and hence the correctness of the extraction of ANC value. In case of the state 8664 keV, which is a subthreshold state, the reproduction of the variation does not follow a purely inverse square dependence. The mismatch is a result of nonreproduction of the tail part of this weakly bound state with the asymptotic radial behavior of the Whittaker function. The values of SPANCs and the corresponding ANCs of the states of $^{23}$Na are listed in Tables II and IV.

### 3. *Uncertainties of extracted ANC values*

The uncertainty of the estimated value of ANC was calculated by propagating the error of the spectroscopic factor through the relation given in Eq. (2). In Fig. 5, extracted ANC with the estimated error is as a function of SPANC $b$. The fit to these secondary data points produces the mean ANC value along with its uncertainty. Besides, the dependence of the extracted ANC on the binding energy of the state was also checked. In Fig. 6, we show the plots of ANC as a function of binding energy [26] for the states at 8664 and 6917 keV excitation energies of $^{23}$Na. Binding energy of a state is varied, keeping fixed the geometry parameters of the bound state potential corresponding to the mean ANC value for the state. The plots show that, unlike the more bound 6917 keV state, the ANC value of subthreshold state 8664 keV decreases with increasing binding energy. Thus for the 8664 keV state the uncertainty of the ANC due to the $\pm 3$ keV [15] uncertainty in the binding energy was estimated graphically from the plot shown in Fig. 6. Uncertainties in the ANCs for other deeply bound states corresponding to the error in the binding energies are negligibly small and are not considered.

### 4. *DWBA calculation for the $E_x = 8945$ keV resonance state*

The state at excitation of 8945 keV in $^{23}$Na is a resonance state about 151 keV above the proton threshold. It has an important contribution in the reaction rate of $^{22}$Ne$(p,\gamma)$ at $T = 0.1$ GK as it falls within the Gamow window at this temperature. In earlier reports [15,27], it was considered that at this excitation a single state exists with generally adopted spin-parity of $7/2^-$. Later Jenkins *et al.* [28] in their $\gamma$ spectroscopic study of $^{23}$Na showed that at this excitation the nucleus has a doublet of states with about a keV difference in excitation energy. One of them has a spin-parity of $J^\pi = 7/2^-$ and decays to $9/2^+$ and $5/2^+$ states of $^{23}$Na by dipole transitions. The assignment is consistent with an $l = 3$ angular momentum transfer from a $(d,n)$ study [29]. On the other hand, the measurement also shows a distinct coincidence of a 3914 keV $\gamma$ ray depopulating the $5/2^+$ state at 3914 keV excitation with a 5030 keV $\gamma$ ray that depopulates the relevant 8944 keV state. A spin-parity of $3/2^+$ was assigned to this second state from its decay branches and angular correlation ratio. In a further study, Kelly *et al.* [12] also observed a strong primary transition from this $3/2^+$ state to the $5/2^+$ 3914-keV state with branching ratio of 80% and to the $1/2^+$ 2391 keV

TABLE V. Angular momentum transfers, spectroscopic factors and proton widths of 8945 MeV state in $^{22}$Ne($^{3}$He, $d$) $^{23}$Na reaction.

| $E_x$ (keV) | $J^\pi$ | $l_p$ | $nl_j$ | $C^2S$ Present | $C^2S$ Literature [15] | $\Gamma_p$ (keV) |
|---|---|---|---|---|---|---|
| 8944 | $3/2^+$ | 2 | $1d_{3/2}$ | $(5.54 \pm 1.41) \times 10^{-4}$ | $8.32 \times 10^{-4}$ | $(9.99 \pm 2.50) \times 10^{-8}$ |
| 8945 | $7/2^-$ | 3 | $1f_{7/2}$ | $(3.94 \pm 0.9) \times 10^{-4}$ | $\leqslant 1.08 \times 10^{-3}$ | $(9.83 \pm 2.24) \times 10^{-10}$ |

state with 20%. Hale *et al.* also performed zero-range DWBA fits to the data of the $^{22}$Ne($^{3}$He, $d$) $^{23}$Na* (8945 MeV) reaction [15] with $l = 1, 2, 3$ angular momentum transfers. They opted for $l = 2$ transfer, assigning a $3/2^+$ spin-parity for the 8945 MeV state.

Although the number of data points in the angular distribution is small, we carried out a reanalysis within the zero-range DWBA framework for this unbound state using the code DWUCK4 code [30]. The same set of potentials from Ref. [15] was used. Values obtained by Hale *et al.* assuming an $l = 3$ transfer and by Kelly *et al.* [12] assuming $l = 2$ were reproduced. Subsequently, we completed a least-squares fit to the angular distribution data assuming that both $l = 2$ ($J^\pi = 3/2^+$) and $l = 3$ ($J^\pi = 7/2^-$) can contribute, and the calculation yielded the spectroscopic factors shown in column 5 of Table V. The fits obtained are compared in Fig. 7. A normalizing constant $N = 4.42$ was used in the zero-range DWBA calculation for ($^{3}$He, $d$) [15,20]. It is apparent from Fig. 7 that the fit obtained considering the contributions of both $l = 2$ and 3 is a better reproduction of the limited angular distribution data available.

The partial widths $\Gamma_p$ were estimated for the doublet states having excitation energy $E_x = 8945$ MeV from the extracted spectroscopic factors using the relation

$$\Gamma_p = (C^2S)\Gamma_{sp}, \tag{4}$$

where $C\ ^2S$ is the spectroscopic factor of the resonant state of $^{23}$Na for the particular configuration and $\Gamma_{sp}$ is single-particle width of the state. The single-particle width $\Gamma_{sp}$ for a pure single-particle configuration depends, like the spectroscopic factor, on the choice of the nuclear potential used to generate the corresponding wave function. To estimate the systematic uncertainty in extracted $\Gamma_p$, we varied the radius and diffuseness parameters of the bound state potential from 1.125 to 1.375 fm and from 0.39 to 0.89 fm, respectively, keeping the binding energy fixed. It is observed that partial width $\Gamma_p$ is more or less independent of the chosen parameters as $C^2S$ and $\Gamma_{sp}$ have opposing trends of dependence on the parameters. In the last column of Table V, the extracted particle widths are listed. The errors shown include the fitting uncertainty as well as the systematic uncertainty. We retained the individual contributions of the doublet pair in the estimation of the rate of the proton capture reaction within the relevant temperature window.

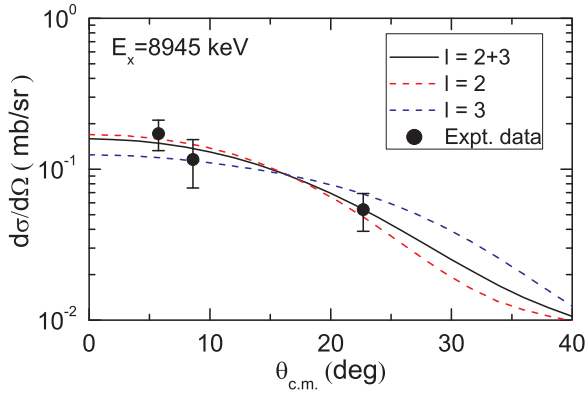


FIG. 7. Angular distribution data and DWBA fits to the 151 keV resonance state of $^{23}$Na.

### B. *R*-matrix calculation for the direct capture process

The low energy behavior of the off-resonance astrophysical $S$ factor for the $^{22}$Ne($p, \gamma$) $^{23}$Na reaction is determined by the direct capture process and a broad subthreshold resonance at 8664 keV in the compound nucleus $^{23}$Na [13]. The present work attempts an $R$-matrix description of the low energy behavior of the off-resonance $S$ factor through the estimation of the direct capture component and the contribution of the subthreshold state constrained by the extracted asymptotic normalization coefficients (ANCs).

The modeling of direct capture in $^{22}$Ne($p, \gamma$) $^{23}$Na is done using the $R$-matrix code AZURE2 [31] based on the basic theory developed in the seminal works of Lane and Thomas [32] and of Vogt [33]. In $R$-matrix modeling, the *channel radius* ($r_c$) divides the radial space into external and internal parts [32]. Accordingly, the capture cross section is divided into an external capture contribution coming from the radial region beyond $r_c$ and an internal capture contribution from the region below $r_c$. The magnitude of the external capture cross section is determined by the *asymptotic normalization coefficient* (ANC) of the final bound state [14,31,34]. The internal capture component of the direct or nonresonant contribution, on the other hand, is simulated by the high energy background states in the composite nucleus [35]. Thus the direct capture part of the cross section is modeled in AZURE2 as a sum of the external capture component and the contribution from high energy background poles.

In the present work, we fitted simultaneously the direct capture data of Rolfs *et al.* and Göress *et al.*. A detailed experimental study of the nonresonant or direct capture component of the reaction $^{22}$Ne($p, \gamma$) $^{23}$Na by Rolfs *et al.* [18] reported the measurement of cross sections for the transitions to six excited states and the ground state of $^{23}$Na for proton energies varying from $E_p = 550$ keV to 2 MeV. In a subsequent experiment, Göress *et al.* [19] remeasured the direct capture cross sections elaborately from $E_p = 550$ keV to 1.6 MeV and also deduced the spectroscopic factors of the final bound states from the fit to the capture data. The data from recent

TABLE VI. Background pole parameters obtained from *R*-matrix fits.

| | | | $\Gamma_\gamma[E1]$ (eV) | | | | | | |
|---|---|---|---|---|---|---|---|---|---|
| $J^\pi$ | $E_x$ (MeV) | $\Gamma_P$ (MeV) | $R \to$ g.s | $R \to 0.44$ | $R \to 2.39$ | $R \to 2.98$ | $R \to 6.30$ | $R \to 6.91$ | $R \to 8.66$ |
| $1/2^-$ | 15 | 5.0 | 589.92 | | $2.77 \times 10^3$ | 499.10 | 912.64 | | 118.42 |
| $1/2^+$ | 15 | 5.0 | | | | | | 4.41 | |
| $3/2^-$ | 15 | 5.0 | | 632.97 | | | | | |

low energy direct or off-resonance capture measurements by Kelly *et al.* [12] at $E_p = 425$ keV and by Ferraro *et al.* [13] at $E_p = 188$, 205, 250, and 310 keV beam energies were also included in the *R*-matrix analysis. Ferraro *et al.* provided *S*-factor data for off-resonance capture to the ground state including the contribution of the decay of the subthreshold resonance at 8664 keV and the total off-resonance *S*-factor data. The new measurements restricted the *R*-matrix model prediction for low energy *S*-factor data for off-resonance capture in $^{22}$Ne$(p,\gamma)\,^{23}$Na.

The channel radius, $r_c$, is fixed at $r_c = 5.5$ fm, a value greater than the nuclear radius of $R_N = 1.25 \times (A_p^{1/3} + A_T^{1/3}) = 4.75$ fm for the $^{22}$Ne$+p$ system. Channel radius is not a parameter in *R*-matrix modeling. A value of $r_c = 5.5$ fm was chosen based on $\chi^2$ minimization employing a grid search technique, keeping the ANCs fixed but varying the parameters of the background poles. The search was performed on the total off-resonance *S*-factor data to choose the radius.

To fit the data for direct capture to individual states and the total off-resonant capture *S* factor simultaneously, we consider $M1$ transitions to states with $J^\pi = 1/2^+$ (*s*-wave capture), $M1 + E2$ transitions to $J^\pi = 3/2^+$, $5/2^+$ (*d*-wave capture), and $M1$ transition to $J^\pi = 1/2^-$ (*p*-wave capture) final bound states. The ANCs for the bound states required for external capture estimates, derived from transfer reaction analysis and listed in Tables II and IV, are kept fixed during the fit to the *S*-factor data. To account for the internal capture component, we introduced high energy background poles in the *R*-matrix analysis. The poles having spin-parity $1/2^+$, $1/2^-$, $3/2^-$ are included and only the $E1$ decay of the background states has been considered. This number of background poles is found to be the minimum to obtain a simultaneous fit to the data set considered. The poles are placed at an excitation energy of 15 MeV [35]. The proton partial width of the poles is fixed at $\Gamma_p = 5$ MeV and it is within the estimated Wigner limit [36] for particle widths at that excitation. However, $\Gamma_\gamma$ values of the background poles are left as free parameters, with initial value taken from the Weisskopf limit for corresponding gamma transitions. The fitted background pole parameters are shown in Table VI. The resultant *R*-matrix fits to the astrophysical $S(E)$ data for direct capture to excited states are shown in Fig. 8. In Fig. 8, the dashed curves represent the contributions of external direct capture to the states. For each state the external contribution was estimated by subtracting the contribution of background poles as the internal contribution from the best fit total direct capture cross section. It is observed that, near threshold states, the external capture process constitutes almost the whole of the direct capture cross section [34].

In the last panel of Fig. 8, it is observed that a better fit to the DC $\to$ 8664 keV capture data is obtained for an ANC of 166 fm$^{-1/2}$ instead of 144 fm$^{-1/2}$ from the transfer calculation. The value and its uncertainty were obtained from simultaneous best fits, with minimum total $\chi^2$, to the DC $\to$ 8664 keV state, 8664 keV $\to$ GS, and the total *S*-factor data. In the multiparameter fit, the background $\Gamma_\gamma$ values are kept free while a grid search is performed over the ANC of the state. The corresponding background pole parameters are listed in Table VI. The condition of simultaneous fitting has reduced the uncertainty in the ANC value. The enhanced ANC corresponds to spectroscopic factor $C^2S = 0.43$ for the state compared to the value of 0.32 that yielded ANC = 144 fm$^{-1/2}$ from the transfer calculation. The higher spectroscopic factor corroborates well the value given by Ferraro *et al.* [13].

In Fig. 9, along with the DC $\to$ GS contribution (black dashed line), we show the contribution from the decay of the 8664 keV subthreshold ($-130$ keV) resonance (blue dashed line). The state decays to the ground state with a branching of $(84 \pm 3)\%$ [37] ($\Gamma_\gamma = 4.7$ eV [27]). The orange solid line in Fig. 9 represents the result from the *R*-matrix fit to total off-resonance capture to the ground state of $^{23}$Na. External direct capture to this state is shown by black dashed-dotted line in Fig. 9. The rise in the low energy *S*-factor data has been nicely reproduced. No interference effect between the two transitions is observed as the summed contribution (pink dashed line) of individual DC $\to$ GS and 8664 keV $\to$ GS coincides with the solid orange line obtained directly. The total $S(E)$ for off-resonance capture in $^{22}$Ne$(p,\gamma)\,^{23}$Na obtained by summing all the individual $S(E)$ functions for transitions to the ground and the excited states is shown in Fig. 10. Excellent overall fits to the data sets are obtained.

The total $S_{\rm tot}^{DC}(0)$ value for direct capture contribution is $48.8 \pm 9.5$ keV b from the present *R*-matrix calculation. The uncertainty in the value includes the contributions from the variation in $r_c$, energy location of background poles, and uncertainty values of the ANCs added in quadrature. The dominant contribution comes from the uncertainty in the ANC of the 8664 keV sub-threshold state. Also a 10% variation in $r_c$ introduces a variation of 6.24 keV b in the total direct capture *S* factor. The present value is close to $S_{tot}^{DC}(0) = (50 \pm 12)$ keV b reported by Ferraro *et al.* [13] but less than the previously adopted value of 62 keV b [14,27]. However, the resultant uncertainty from the present estimation is less.

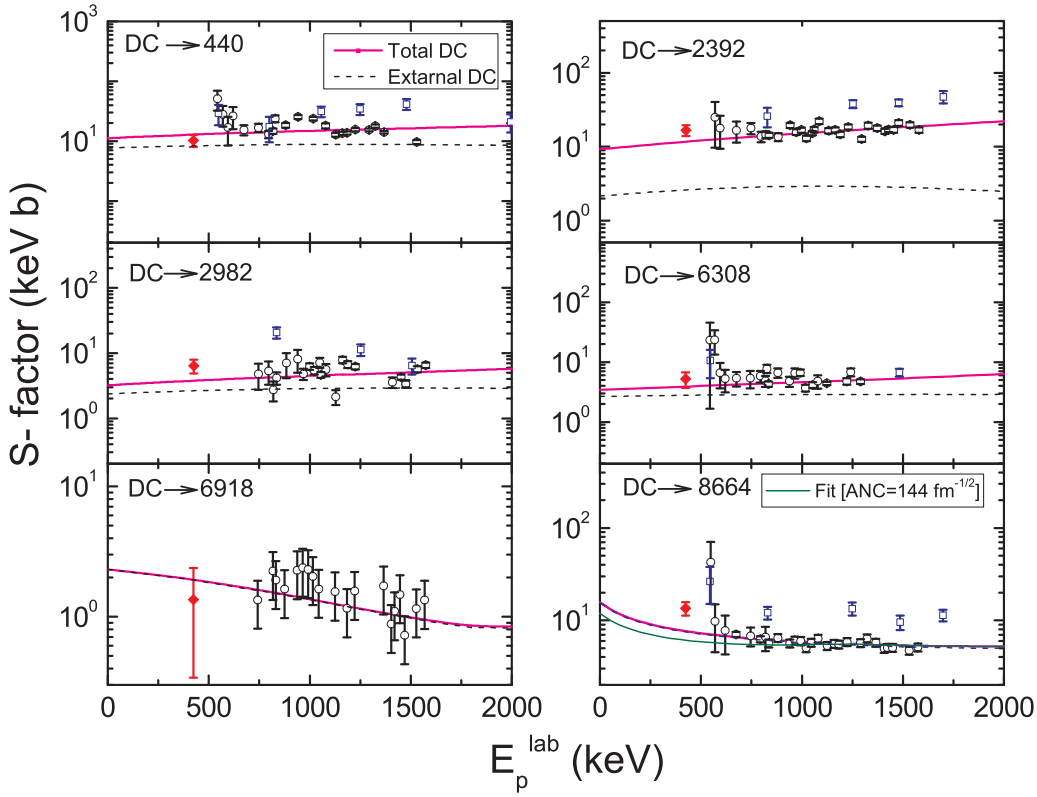


FIG. 8. *R*-matrix fit to the *S*-factor curve for direct capture to six bound states of $^{23}$Na. The red solid curves are the *R*-matrix fits with the contribution of background poles while the dashed curves represent the calculation without the background poles. The panel showing the *S*-factor curve for the DC → 8664 keV subthreshold state also includes the *R*-matrix fit (green dashed curve) with ANC value fixed from the transfer reaction calculation. The solid curve in this panel depicts the *R*-matrix fit with ANC value of 166 fm$^{-1/2}$ for the state.

## III. THERMONUCLEAR REACTION RATE OF $^{22}$Ne($p$, $\gamma$) $^{23}$Na

The thermonuclear reaction rate of $^{22}$Ne$(p, \gamma)$ $^{23}$Na is controlled by several noninterfering low energy narrow resonances and the total off-resonance capture reaction. The reaction rate for narrow resonances is calculated using the analytical expression

$$N_A\langle\sigma\upsilon\rangle = \sqrt[3]{\left(\frac{2\pi}{\mu kT}\right)}\hbar^2(\omega\gamma)_r \exp\left(-\frac{E_r}{kT}\right). \quad (5)$$

The quantity $\mu$ is the reduced mass, $k$ is Boltzmann's constant, $E_r$ is resonance energy in the center-of-mass frame, and $\omega\gamma$ is the resonance strength with $\omega$ being the statistical spin

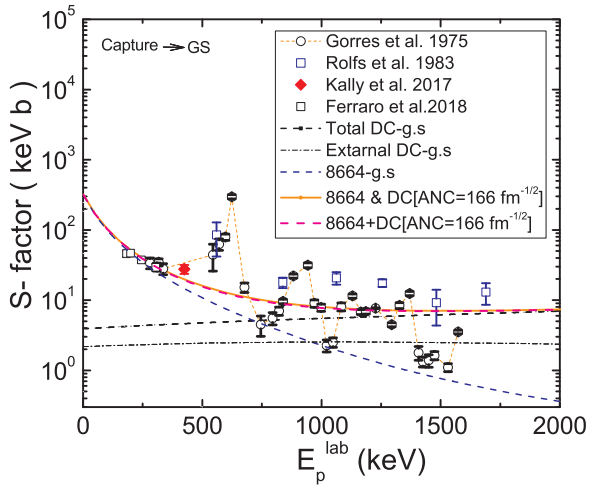


FIG. 9. *R*-matrix fit to the data of direct capture to the ground state of $^{23}$Na.

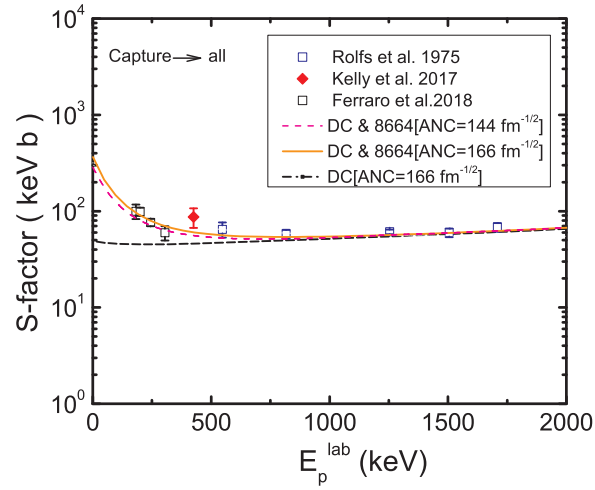


FIG. 10. *R*-matrix fit to the data of total direct capture in $^{23}$Na.

TABLE VII. Summary of resonance strengths ($\omega\gamma$) used in reaction rate estimation.

| $E_x$ (keV) | $E_r$ (keV) | $\omega\gamma$ (keV)[a] Literature | $\omega\gamma$ (keV) Present |
|---|---|---|---|
| 8830 | 35 | $(3.6 \pm 0.2) \times 10^{-15}$ [15] | |
| 8862 | 68 | $\leqslant 6 \times 10^{-11}$ [13] | |
| 8894 | 100 | $\leqslant 7.0 \times 10^{-11}$ [13] | |
| 8945 | 151 | $2.7 \times 10^{-7}$ [13] | $(2.0 \pm 0.5) \times 10^{-7}$ |
| | | $2.03 \times 10^{-7}$ [12] | |
| 8944 | 150 | $\leqslant 9.7 \times 10^{-8}$ [12] | $(3.93 \pm 0.9) \times 10^{-9}$ |
| 8972 | 178 | $(2.7 \pm 0.2) \times 10^{-6}$ [13] | |
| 9000 | 205.6 | $\leqslant 2.8 \times 10^{-8}$ [8] | |
| 9042 | 248.4 | $(9.7 \pm 0.7) \times 10^{-6}$ [13] | |
| 9211 | 417 | $(8.8 \pm 1.02) \times 10^{-2}$ [12] | |
| 9252 | 458 | 0.5 [38] | |

[a]Resonance strengths of states with $E_r$ above 458 keV are taken from the STARLIB Compilation [17].

factor and $\gamma = \frac{\Gamma_p \Gamma_\gamma}{\Gamma}$, where $\Gamma_p$, $\Gamma_\gamma$, and $\Gamma$ are the proton partial width, $\gamma$ decay width, and the total width, respectively. Resonance strengths used in the estimation are listed in Table VII. Only the strengths of the doublet states around $E_r = 151$ keV were determined in the present work, and the corresponding summed contribution is shown by the green solid line in the figure. In estimating the reaction rate, all the resonance strengths were divided by the calculated electron screening enhancement factor corresponding to the respective excitation energy and tabulated in Table I of Ref. [13]. The rates plotted for $E_r = 68$ and 100 keV were calculated with only the experimental upper limits of the respective resonance strengths reported by Ferraro *et al.* [13]. The $S_{tot}(E)$, yielded by the *R*-matrix calculation for the total DC plus subthreshold contribution to the ground state, was used to get the rate for the off-resonant component (black solid line in the upper panel). The uncertainty limits of the off-resonant contribution (black dashed-dotteed line) were calculated from the total uncertainty in the off-resonant astrophysical *S* factor. Individual components are shown in the upper panel of Fig. 11. The nonresonant reaction rates were determined using the code EXP2RATE V2.1 by Rauscher [39].

The total rate, which is the sum of all individual components, is indicated by a bold red line in the lower panel of Fig. 11. Based on their estimation of the upper limits of 68 and 100 keV resonance strengths, Ferraro *et al.* assumed that the role of these resonances in the total rate at the relevant temperature is insignificant. To compare our total rate in the same temperature window with those of Ferraro *et al.*, Hale *et al.*, and Cavanna *et al.*, we estimated the total rate without the contributions of 68 and 100 keV resonances. Around $T = 0.1$ GK, the present rate is about an order higher than Hale's rate but only slightly higher compared to the rates determined by Cavanna *et al.* as well as Ferraro *et al.*. For the $0.1 \leqslant T \leqslant 0.2$ GK region, the estimated rate is distinctly higher than both the other rates. In the $T \leqslant 0.1$ GK region, our rate is similar to the rate obtained by Ferraro *et al*. The associated upper and lower uncertainty limits are shown by red dashed lines. While calculating the limits for the resonant capture rate, we took into account the uncertainties of the energy locations of states along with respective uncertainties of the resonance strengths. While the upper limits of the strengths of 68 and 100 keV resonances are considered in estimating the upper limit of total rate, for the lower limit of the total rate the lower limits of the strengths are set to zero [9]. Thus the effect of 68 and 100 keV resonances is included in the uncertainty region of the total rate bounded by the red dashed lines.

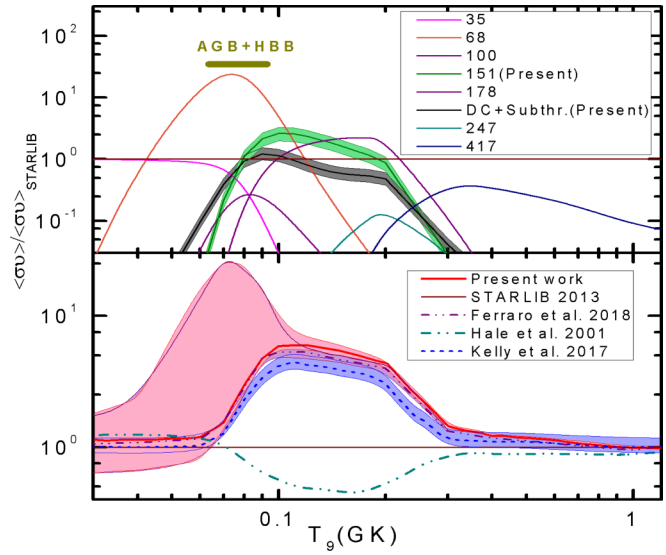


FIG. 11. Ratio of reaction rate from present calculation to the STARLIB rate for direct and resonant captures in the $^{22}$Ne$(p, \gamma)$ $^{23}$Na reaction. The solid curve represents the ratio with the total capture rate of the reaction.

## IV. CONCLUSION

A consistent analysis of the direct capture reaction in $^{22}$Ne$(p, \gamma)$ $^{23}$Na was performed within the *R*-matrix framework, constrained with the asymptotic normalization constants of the bound states of $^{23}$Na obtained from the transfer reaction calculation. Asymptotic normalization constants were extracted from finite DWBA analysis of $^{22}$Ne$(^3$He$, d)$ $^{23}$Na transfer data.

Astrophysical *S*-factor data for capture to the bound states of $^{23}$Na were reproduced from the analysis. The contribution of capture through the subthreshold resonance at 8664 keV excitation in the total capture to the ground state of $^{23}$Na was delineated. The observed rise in the ground sate capture data was reproduced nicely. The total direct capture *S* factor at zero relative energy, $S_{DC}(0)$, was found to be $48.8 \pm 9.5$, having less uncertainty.

The total reaction rate obtained as a function of temperature differs from the recent estimations by Ferraro *et al.* in the temperature window of $0.1 \leqslant T \leqslant 0.2$ GK. The difference is due to slightly higher contribution from direct plus subthreshold capture to the ground state. However, the present uncertainty in the total rate in this region is relatively higher due to the uncertainty in the resonance strength of the unbound state extracted from transfer angular distribution data. However, for $T \leqslant 0.1$ GK, the uncertainty in the rate is comparable with the result of Ferraro *et al*.

[1] R. M. Cavallo, A. V. Sweigart, and R. A. Bell, Astrophys. J. **492**, 575 (1998).
[2] P. L. Cottrell and G. S. Da Costa, Astrophys. J. **245**, L79 (1981).
[3] C. A. Pilachowski, Astrophys. J. **326**, L57 (1988).
[4] G. Paltoglou and J. E. Norris, Astrophys. J. **336**, 185 (1989).
[5] E. Carretta, S. Lucatello, R. G. Gratton, A. Bragaglia, and V. D'Orazi, Astron. Astrophys. **533**, A69 (2011).
[6] K. Lind, C. Charbonnel, T. Decressin, F. Primas, F. Grundahl, and M. Asplund, Astron. Astrophys. **527**, A148 (2011).
[7] D. Yong, F. Grundahl, D. L. Lambert, P. E. Nissen, and M. D. Shetrone, Astron. Astrophys. **402**, 985 (2003).
[8] F. Cavanna (The LUNA Collaboration), Phys. Rev. Lett. **115**, 252501 (2015).
[9] R. Depalo *et al.* (LUNA Collaboration), Phys. Rev. C **94**, 055804 (2016).
[10] F. Cavanna (The LUNA Collaboration), Phys. Rev. Lett. **120**, 239901(E) (2018).
[11] D. Bremmer *et al.*, Europhys. Lett. **122**, 52001 (2018).
[12] K. J. Kelly, A. E. Champagne, L. N. Downen, J. R. Dermigny, and S. Hunt, C. Iliadis, and A. L. Cooper, Phys. Rev. C **95**, 015806 (2017).
[13] F. Ferraro, M. P. Takács, D. Piatti, F. Cavanna *et al.*, Phys. Rev. Lett. **121**, 172701 (2018).
[14] C. Angulo, M. Arnould, M. Rayet, P. Descouvemont *et al.*, Nucl. Phys. A **656**, 3 (1999).
[15] S. E. Hale, A. E. Champagne, C. Iliadis, V. Y. Hansper, D. C. Powell, and J. C. Blackmon, Phys. Rev. C **65**, 015801 (2001).
[16] C. Iliadis, R. Longland, A. E. Champagne, A. Coc, and R. Fitzgerald, Nucl. Phys. A **841**, 31 (2010).
[17] A. L. Sallaska, C. Iliadis, A. E. Champange, S. Goriely, S. Starrfield, and F. X. Timmes, Astrophys. J. Suppl. Ser. **207**, 18 (2013).
[18] C. Rolfs, W. S. Rodney, M. H. Shapiro, and H. Winkler, Nucl. Phys. A **241**, 460 (1975).
[19] J. Görres, H. W. Becker, L. Buchmann, C. Rolfs, P. Schmalbrock, H. P. Trautvetter, and A. Vlieks, Nucl. Phys. A **408**, 372 (1983).
[20] J. R. Powers, H. T. Fortune, R. Middleton, and O. Hansen, Phys. Rev. C **4**, 2030 (1971).
[21] I. J. Thompson, Comput. Phys. Rep. **7**, 167 (1988).
[22] P. Bém, V. Burjan, V. Kroha, J. Novák, Š. Piskoř, E. Šimečkovă, J. Vincour, C. A. Gagliardi, A. M. Mukhamedzhanov, and R. E. Tribble, Phys. Rev. C **62**, 024320 (2000).
[23] I. J. Thompson and F. M. Nunes, *Nuclear Reactions for Astrophysics* (Cambridge University Press, Cambridge, 2009).
[24] D. Y. Pang and A. M. Mukhamedzhanov, Phys. Rev. C **90**, 044611 (2014).
[25] A. Terakawa *et al.*, Phys. Rev. C **48**, 2775 (1993).
[26] N. Keeley, K. W. Kemper, and K. Rusek, Eur. Phys. J. A **54**, 71 (2018).
[27] J. Görres, C. Rolfs, P. Schmalbrock, H. P. Trautvetter, and J. Keinonen, Nucl. Phys. A **385**, 57 (1982).
[28] D. G. Jenkins, M. Bouhelal, S. Courtin, M. Freer, B. R. Fulton, F. Haas, R. V. F. Janssens, T. L. Khoo, C. J. Lister, E. F. Moore, W. A. Richter, B. Truett, and A. H. Wuosmaa, Phys. Rev. C **87**, 064301 (2013).
[29] W. A. Childs, R. C. Ritter, B. D. Murphy, and R. M. Strang, Nucl. Phys. A **203**, 133 (1973).
[30] P. D. Kunz, program DWUCK4 (unpublished) https://www.oecd-nea.org/tools/abstract/detail/nesc9872; extended version of J. R. Comfort (unpublished).
[31] R. E. Azuma, E. Uberseder, E. C. Simpson, and C. R. Brune *et al.*, Phys. Rev. C **81**, 045805 (2010).
[32] A. Lane and R. Thomas, Rev. Mod. Phys. **30**, 257 (1958).
[33] E. Vogt, Rev. Mod. Phys. **34**, 723 (1962).
[34] P. Descouvemont and D. Baye, Rep. Prog. Phys. **73**, 036301 (2010).
[35] A. Kontos, J. Görres, A. Best, M. Couder, R. deBoer, G. Imbriani, Q. Li, D. Robertson, D. Schürmann, E. Stech, E. Uberseder, and M. Wiescher, Phys. Rev. C **86**, 055801 (2012).
[36] C. Rolfs and W. S. Rodney, *Cauldrons in the Cosmos* (Universityof Chicago Press, Chicago, 1988).
[37] R. B. Firestone, Nucl. Data Sheets **108**, 1 (2007).
[38] M. A. Meyer and J. J. A. Smit, Nucl. Phys. A **205**, 177 (1973).
[39] T. Rauscher, EXP2RATE V2.1, https://nucastro.org